

Wetlands of Greater Bangalore, India: Automatic Delineation through Pattern Classifiers

T. V. Ramachandra <cestvr@ces.iisc.ernet.in>
Indian Institute of Science, Bangalore, India
Uttam Kumar <uttam@ces.iisc.ernet.in>
Indian Institute of Science, Bangalore, India

.....

Wetlands are the most productive and biologically diverse but very fragile ecosystems. They are vulnerable to even small changes in their biotic and abiotic factors. In recent years, there has been concern over the continuous degradation of wetlands due to unplanned developmental activities. This necessitates inventorying, mapping, and monitoring of wetlands to implement sustainable management approaches. The principal objective of this work is to evolve a strategy to identify and monitor wetlands using temporal remote sensing (RS) data. Pattern classifiers were used to extract wetlands automatically from NIR bands of MODIS, Landsat MSS and Landsat TM remote sensing data. MODIS provided data for 2002 to 2007, while for 1973 and 1992 IR Bands of Landsat MSS and TM (79m and 30m spatial resolution) data were used. Principal components of IR bands of MODIS (250 m) were fused with IRS LISS-3 NIR (23.5 m). To extract wetlands, statistical unsupervised learning of IR bands for the respective temporal data was performed using Bayesian approach based on prior probability, mean and covariance. Temporal analysis of wetlands indicates a sharp decline of 58% in Greater Bangalore attributing to intense urbanization processes, evident from a 466% increase in built-up area from 1973 to 2007.

Introduction

Wetlands are an essential part of human civilization, meeting many crucial needs for life on earth such as drinking water, protein production, energy, fodder, biodiversity, flood storage, transport, recreation, and climate stabilizers. They also aid in improving water quality by filtering sediments and nutrients from surface water. Wetlands play a major role in removing dissolved nutrients such as nitrogen and to some extent heavy metals (Ramachandra, 2002). They are becoming extinct due to manifold reasons, including anthropogenic and natural processes. Burgeoning populations, intensified human activity, unplanned development, absence of management structures, lack of proper legislation, and lack of awareness about the vital role played by these ecosystems are the important causes that have contributed to their decline and loss. Identifying, delineating, and mapping of wetlands on a temporal scale provide an opportunity to monitor the changes, which is important for natural resource management and planning activities (Ramachandra, Kiran, & Ahalya, 2002). Temporal RS data coupled with spatial analysis helps in monitoring the status and extent of spatial features. The spectral signature associated in each pixel of the remotely sensed data is used to perform the classification and, indeed, is used as the numerical basis for categorization of various spatial features (Lillesand & Kiefer, 2002). Most of these classifications are based on certain pattern recognition techniques. Among the various frameworks in which pattern recognition has been traditionally formulated, the statistical approach has been most intensively studied and used in practice. The design of a recognition system also involves the following issues: definition of pattern classes, sensing environment, pattern representation, feature extraction and selection, cluster analysis, classifier design and learning,

selection of training and test samples, and performance evaluation. Pattern recognition techniques such as neural network, decision tree, fuzzy theory, etc. have been widely used with RS data to identify the patterns in land use classes like urban, agriculture land, etc (Kwan & Cai, 1994), (Fukushima, 1998), (Gori & Scarselli, 1998) and (Lee, Liu, & Chen, 2006). One of the primary applications of pattern classification is feature extraction. Extraction of land cover features of interest from remotely sensed data leads to a number of applications for decision makers to management planners. Given an image, the classifiers can be used to categorize the image into user defined types or to identify features based on their inherent patterns. This paper focuses on identification of wetlands using unsupervised pattern classifiers.

Extracting spatial features such as wetlands (which include lakes, ponds, tanks, marshy areas, etc.) from temporal RS data helps in monitoring their status including spatial extent, physical, chemical, and ecological aspects. Traditional approaches are digitizing through visual investigation, applying a density slicing method or an edge detection method to a single band, and classification using multiple bands (Kevin & El Asmar, 1999). Among these approaches, density slicing is one of the most popular and effective methods with an appropriate threshold. However, it is often difficult to determine the threshold as in the case of Landsat Thematic Mapper (TM) band 4, if the turbidity is very high.

The utility of threshold precipitation in predicting inundation was tested with detailed field investigations to delineate the watershed and determine elevation-bounded intervals based on soil and vegetation types and densities (French, Miller, Dettling, & Carr, 2006). Landsat images in the IR bands have been used to determine the spatial change of water over a defined temporal resolution. Image subtraction followed by binary thresholding was used to extract the exact amount of change in surface water. Threshold precipitation was then compared to precipitation events that occurred within the temporal resolution of the image subtractions to determine the association between precipitation and the inundation of the lake. Near-infrared spectroscopy has been attempted by Czarnik-Matusewicz and Pilorz (2006) to monitor the properties of systems for which water is a major constituent. To distinguish flat, uniform water bodies and cloud or mountain shadows, Wilson (1997) used variance filter as a textural algorithm (TA). Output of TA was a set of rules used by a knowledge based classifier.

In this work, pattern classifiers based on unsupervised learning have been used to extract wetlands from IR Bands of temporal RS data of various spatial resolutions. The maximum likelihood (ML) estimation followed by a Bayesian classifier was employed to quantify the tradeoffs between various classification decisions using probabilistic model. This approach is useful in the smart processing and in automatic extraction of features of interest. The probabilities, mean, and covariance are estimated for the number of user specified classes and based on these a pixel is assigned to a group. The groups are then interpreted based on prior knowledge and field experience. In this method computational complexity increases with varied parametric assumptions (Duda, Hart, & Stork, 2000).

Objective

The objective of this study is to carry out spatial and temporal analysis of wetlands (changes during the period 1973-2007) in Greater Bangalore using IR data through pattern classifiers and to understand responsible causal factors and the likely implication of these dynamics.

Material and Methods **Study Area**

Greater Bangalore (77°37'19.54" E and 12°59'09.76" N) is the principal administrative, cultural, commercial, industrial, and knowledge capital of the state of Karnataka with an area of 741 square kilometres that lies between the latitudes 12°39'00" to 13°3'00"N and longitude 77°22'00" to 77°52'00"E. Bangalore city administrative jurisdiction was widened in 2006 by merging the existing area of Bangalore City spatial limits with eight neighboring Urban Local

Bodies (ULBs) and 111 Villages of Bangalore Urban District (Sudhira, Ramachandra, & Bala Subramanya, 2007). Thus, Bangalore has grown spatially more than ten times since 1949 (69 square kilometres) and is a part of both the Bangalore urban and rural districts (Figure 1). Now, Bangalore is the fifth largest metropolis in India currently with a population of about seven million. The mean annual total rainfall is about 880 mm with about 60 rainy days a year over the last ten years. The summer temperature ranges from 18 °C – 38 °C, while the winter temperature ranges from 12 °C – 25 °C. Thus, Bangalore enjoys a salubrious climate all year round. Bangalore is located at an altitude of 920 metres above mean sea level, delineating four watersheds: Hebbal, Koramangala, Challaghatta and Vrishabhavathi watersheds. The undulating terrain in the region has facilitated creation of a large number of tanks for traditional uses such as irrigation, drinking, fishing, and washing. This led to the existence of hundreds of such water bodies in the past centuries of Bangalore. Even in early second half of the 20th century, in 1961, the number of lakes and tanks in the city stood at 262 (and the spatial extent of Bangalore was 112 square kilometres) and in 1985, the number of lakes and tanks was 81 (and the spatial extent of Bangalore was 161 square kilometres).

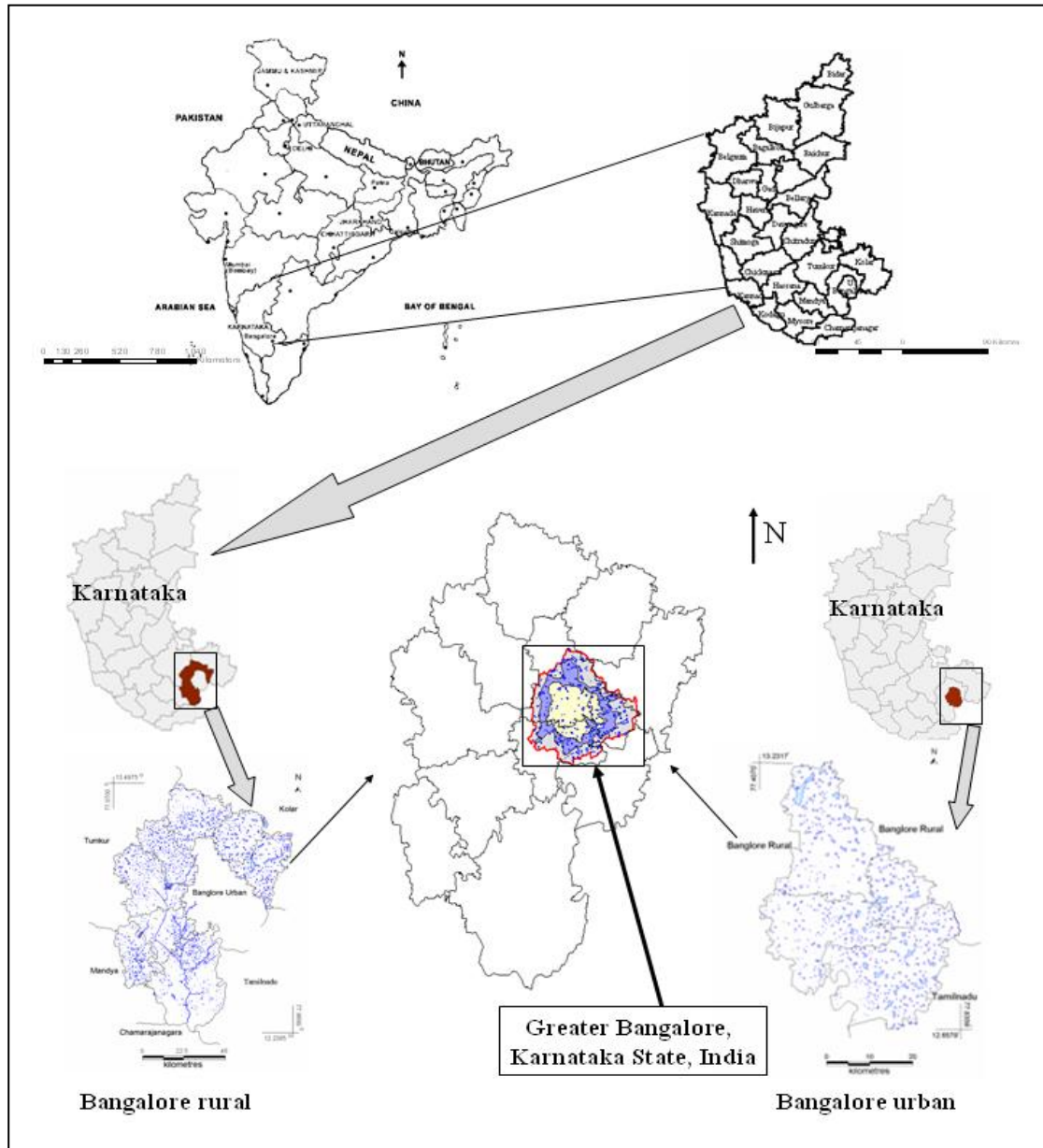


Figure 1. Study area – Greater Bangalore

Data

Survey of India (SOI) toposheets of 1:50000 and 1:250000 scales were used to generate base layers of taluk boundaries, city boundary, drainage networks, and wetlands (Figure 1). Field data were collected with a handheld GPS. RS data used for the study are:

- Landsat MSS data of 1973 (79 m), Landsat TM of 1992 (30 m) [downloaded from <http://glcf.umd.edu/data/>]
- MODIS 7 bands product of 2002 and 2007 (Band 1 and 2 = 250 m and Band 3 to 7 = 500m) [downloaded from <http://edcdaac.usgs.gov/main.asp>]
- IRS LISS-3 (23.5 m) data of 2006 procured from NRSA, Hyderabad, India
- Google Earth data (<http://earth.google.com>) served in pre and post classification process and validation of the results
- Landsat ETM+ (8 bands) of 2000

- SRTM (Shuttle Radar Topography Mission) elevation data of 90 m [downloaded from <http://glcf.umiacs.umd.edu/data/>]

To map wetlands, IR bands are appropriate as water entirely absorbs the energy in wavelengths (0.7–2.35 μm). Suitability of IR bands to extract water line was done successfully by Yamano, H., et al., (2006). The ability of five satellite sensor bands (IKONOS band 4, Terra ASTER bands 3 and 4, and Landsat ETM+ bands 4 and 5) were examined to extract the waterline at coral reef coasts using different wavelength regions (near infrared [NIR] and shortwave infrared [SWIR]) and different spatial resolutions (4, 15, and 30 m). After performing geo-referencing and normalization of images, density slicing was used to extract the waterline. Extracted waterline positions were compared with ground-level data of the island shorelines for eight transects using global positioning system (GPS).

Methods

The methods adopted in the analysis involved:

1. Creation of base layers like district boundary, district with taluk and village boundaries, road network, drainage network, mapping of water bodies, etc. from the SOI toposheets of scale 1:250000 and 1:50000.
2. Geo-referencing of acquired RS data to latitude-longitude coordinate system with Evrst 56 datum: Landsat bands, MODIS bands 1 and 2 (spatial resolution 250 m) and bands 3 to 7 (spatial resolution 500 m) were geo-corrected with the known ground control points (GCP's). Re-projection from Sinusoidal to Polyconic with Evrst 1956 as the datum, followed by masking and cropping of the study area.
3. Re-sampling using nearest neighborhood technique:
 - NIR and MIR bands (bands 3 and 4) of Landsat 1973 data to 23.5 m.
 - 3 IR bands of Landsat (band 4-NIR, 5-MIR and 7-MIR) of 1992 to 23.5 m.
 - 4 IR MODIS bands 2 and 5 to 7 (MOD 09 product) to 250 m.
4. Principal Component Analysis (PCA): Principal components representing maximum variability of the original datasets were chosen based on eigen values with PCA (given in Appendix A) of MODIS bands 2, 5, 6 and 7.
5. Principal components of MODIS data (250 m spatial resolution) were fused with IR Band (Band 3) of IRS LISS-3 MSS data (23.5 m spatial resolution) using RGB – HIS algorithm (Carper, Lillesand, & Kiefer, 1990) as discussed in Appendix B. The three principal components (PC1, PC2 and PC3) of the low resolution MODIS were transformed to IHS (I is intensity, H is hue, S is saturation). I was replaced with the IR band of LISS-3 (of spatial resolution 23.5 m). Then, the fused images were obtained by performing an inverse transformation of IHS back to the original RGB.
6. K-means algorithm was used to partition the data samples in the feature space into disjoint subsets or clusters as discussed in Appendix C. The similarity between two data points was quantified using a distance measure that facilitates measurement of the clustering quality of a partition. Pixels were clustered into 4 groups – built-up, vegetation, wetlands and others (based on field knowledge) based on randomly chosen 4 seed pixels.
7. The prior probability $P(\omega_k)$ for the k^{th} class which is the proportion of the number of pixels in that class to the total number of pixels and the covariance matrix Σ_k were computed. A pixel was assigned to a particular class for which it has the maximum probability (details in Appendix D).
8. Accuracy assessment of automatically extracted wetlands was done with field knowledge, visual interpretation and also referring Google Earth (<http://earth.google.com>).

Results and Discussion

In unsupervised learning, where no previous estimation parameters were available, quite motivating and realistic results were obtained in extracting water bodies and their extent using IR bands of RS data. The corresponding number of wetlands and their areas were computed and are listed in Table 1. Figure 2 provides the distribution of wetlands in 1973, 1992, 2002, and 2007

based on the respective years' RS data. The analysis revealed that there were 51 wetlands (321 ha) in 1973, 38 (207 ha) in 1992, 25 (135 ha) in 2002 and the number of wetlands dropped down to 17 with an extent of 87 ha in 2007 in the Bangalore city limits.

Table 1. Status of water bodies in Bangalore city limits and Greater Bangalore

| | Bangalore City | | Greater Bangalore | |
|------|------------------------|--------------|------------------------|--------------|
| | Number of Water bodies | Area (in ha) | Number of Water bodies | Area (in ha) |
| SOI | 58 | 406 | 207 | 2342 |
| 1973 | 51 | 321 | 159 | 2003 |
| 1992 | 38 | 207 | 147 | 1582 |
| 2002 | 25 | 135 | 107 | 1083 |
| 2007 | 17 | 87 | 93 | 918 |

Note: SOI, Survey of India topographic maps (published in 1973)

There were 159 water bodies spread in an area of 2003 ha in 1973, that number declined to 147 (1582 ha) in 1992, which further declined to 107 (1083 ha) in 2002, and finally there are only 93 water bodies (both small and medium size) with an area of 918 ha in the Greater Bangalore region in 2007. Water bodies in the northern part of greater Bangalore are in a considerably poor state compared to the wetlands in southern greater Bangalore. Validation of the classified data was done through field visits during July 2007, which indicate an accuracy of 91%. The error of omission was mainly due to the cover of water hyacinth (aquatic macrophytes) in water bodies due to which the energy was reflected in IR bands rather than getting absorbed. Fifty-four water bodies were sampled through field visits while the remaining water bodies were verified using online Google Earth (<http://earth.google.com>).

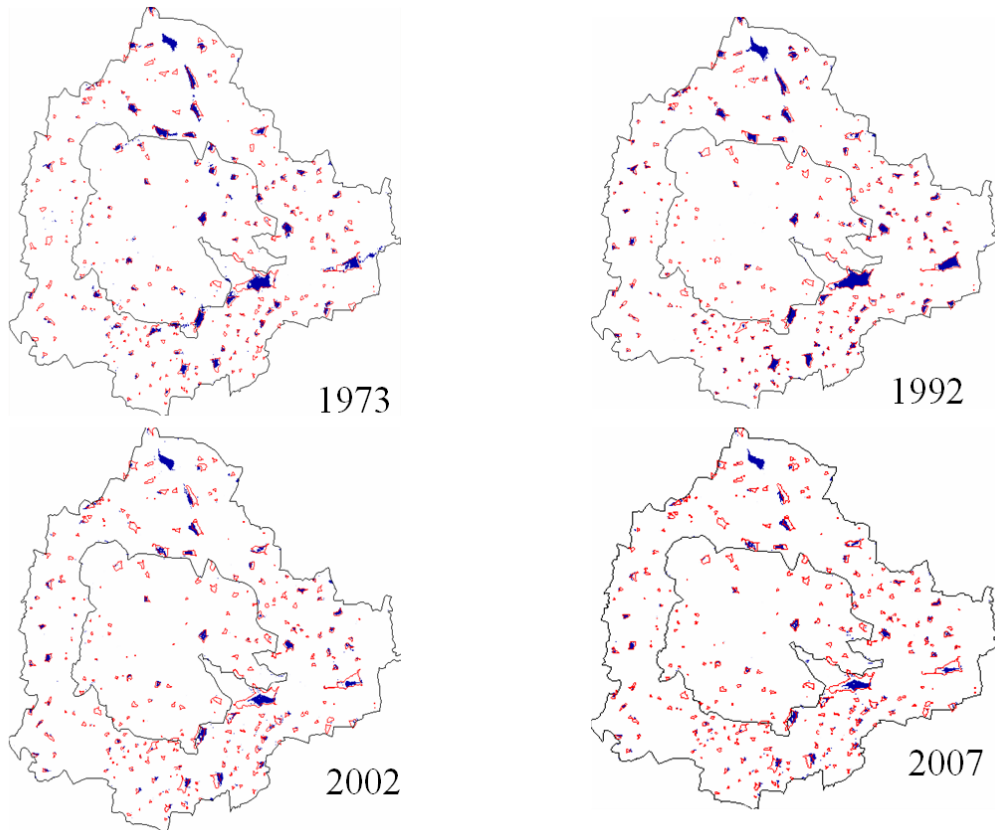


Figure 2. Unsupervised learning to extract water bodies from NIR bands. Water bodies are represented in blue and the vector layer of water bodies generated from SOI Toposheet is overlaid (in red) that exactly fits on the existing water bodies. The inner boundary (in black) is the Bangalore city limit and the outer boundary represents the spatial extent of Greater Bangalore.

Temporal analyses indicate the decline of 34.48% during 1973 to 1992, 56.90% during 1973-2002 and 70.69% during 1973-2007 in the erstwhile Bangalore city limits. Similar analyses done for Greater Bangalore (i.e. Bangalore city with surrounding 8 municipalities) indicate the decline of 32.47% during 1973 to 1992, 53.76% during 1973-2002 and 60.83% during 1973-2007. This is correlated with the increase in built-up area from the concentrated growth model focusing on Bangalore, adopted by the state machinery, affecting severely open spaces and in particular water bodies. Some of the lakes have been restored by the city corporation and the concerned authorities in recent times. These lakes have a well defined boundary, clean water and are maintained by the neighborhood people. These lakes are used for recreational purposes. They are home to migratory birds and also add aesthetic beauty to the surroundings.

Disappearance of water bodies and a sharp decline in the number of water bodies in Bangalore is mainly due to intense urbanization and urban sprawl. Many lakes were encroached for illegal buildings (54%). Field surveys (during July-August 2007) show that nearly 66% of lakes are sewage fed, 14% surrounded by slums and 72% showed loss of catchment area. Also, lake catchments were used as dumping yards for either municipal solid waste or building debris. The areas surrounding these lakes have illegal constructions of buildings and most of the time slum dwellers occupy the adjoining areas. At many sites, water is used for washing and household activities and even fishing was observed at one of these sites. Multi-storied buildings have come

up on some lake beds that have totally intervened with the natural catchment flow leading to a sharp decline in the catchment yield and also a deteriorating quality of water bodies. Figure 3 gives the land use categories in Greater Bangalore obtained by classifying Landsat ETM+ data. This highlights the intense urbanization process in the core city.

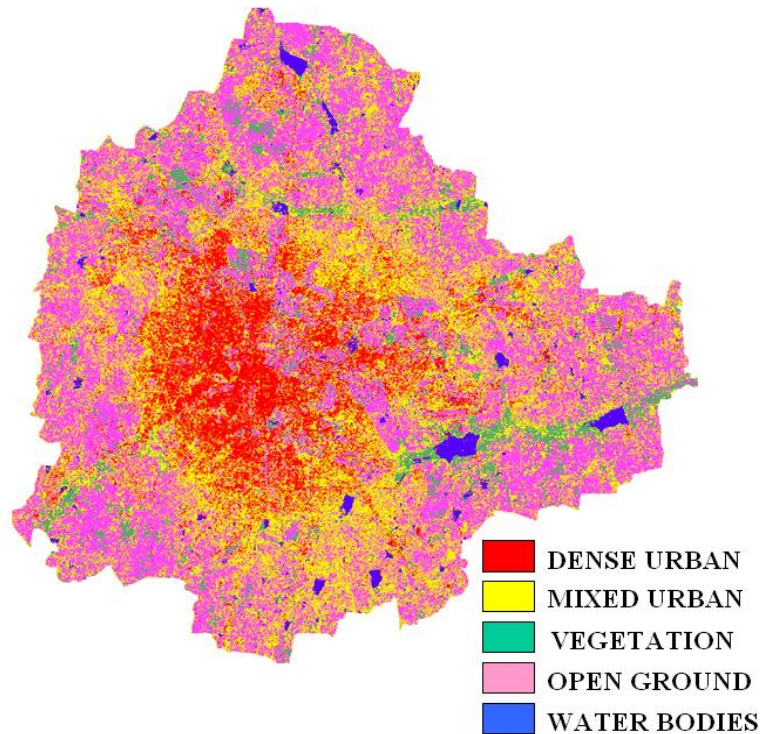


Figure 3. Land use in Greater Bangalore obtained from Landsat ETM+

Temporal analysis of land use show that there has been a 466% increase in built-up area from 1973 to 2007 leading to a sharp decline in water bodies (60.83%) in Greater Bangalore. Figure 4 illustrates the rate of increase in built-up areas from 1973 to 2007 and its implication on the decline of vegetation and water bodies. Vegetation has decreased by 32% from 1973 to 1992, by 38% from 1992 to 2002 and by 63% from 2002 to 2007. Figure 5 shows the relation found between impermeable areas to urban population density, indicating the increase in population with the increase in paved surface in the region. Unplanned urbanization has many potentially detrimental effects including the loss of valuable agricultural and eco-sensitive (e.g. wetlands, forests) lands, enhanced energy consumption and greenhouse gas emissions from increasing private vehicle use.

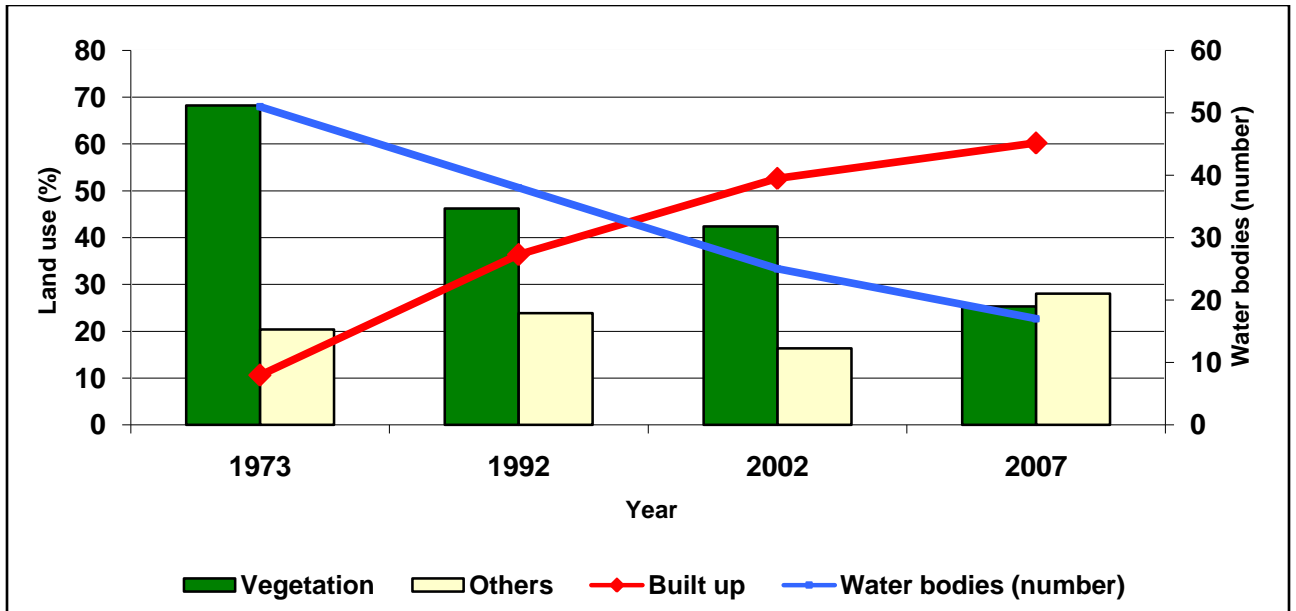


Figure 4. Impact of urbanization on vegetation and water bodies

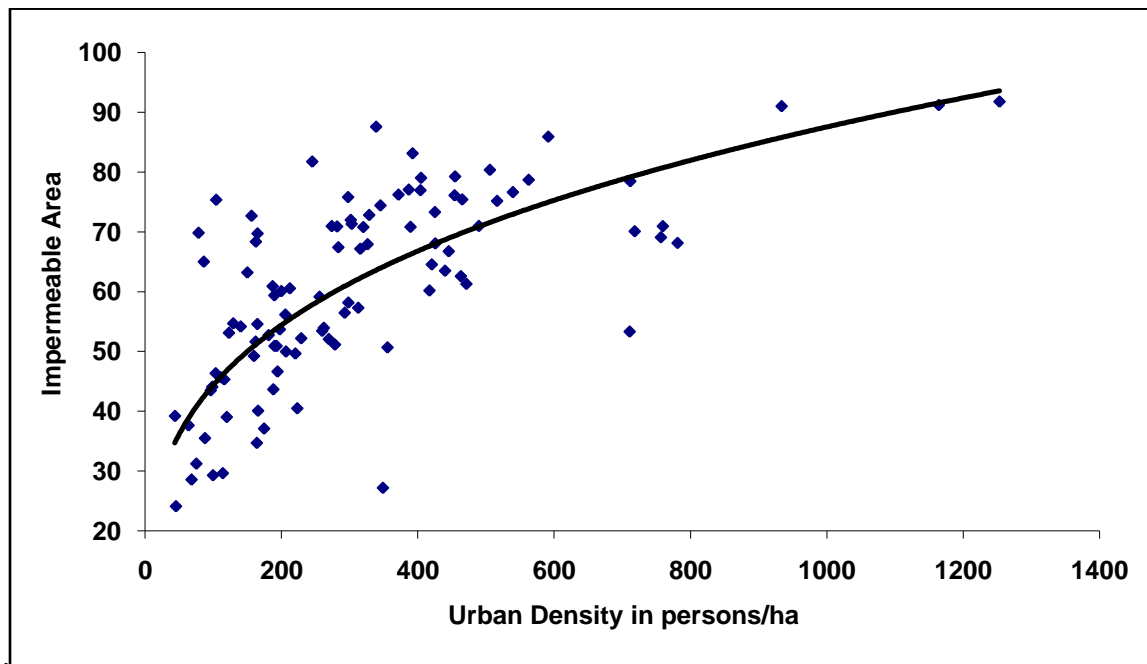


Figure 5. Impermeable area and urban density in Bangalore city

Urbanization and the consequent loss of lakes has led to decreases in catchment yield, water storage capacity, wetland area, number of migratory birds, flora and fauna diversity and ground water table. Studies in selected lake catchments in Bangalore reveal the decrease in depth of the ground water table from 10-12m to 100-200m in 20 years due to the disappearance of wetlands.

Reclamation of lakes for various developmental activities has resulted in the loss of interconnectivity in Bangalore district leading to higher instances of floods even during the normal rainfall. Analyses of Bellandur and Ulsoor drainage network (Figure 6) showed that the network is lost due to conversion of Chelgatta tank into a golf course. Ulsoor – Bellandur catchment has six

lakes – Sankey, Ulsoor, Chalghata, Chinnagara and Varthur and was classified into three major land use types – built-up, vegetation, and others (comprising open land, waste land etc). The total rainfall yield in this catchment is 240Mm^3 , percolated water is 90Mm^3 and water overflow is 150Mm^3 . The SRTM DEM data were re-sampled to 10m resolution and the volume of each lake was computed assuming the depth to be 1m and the mean annual rainfall to be 850mm. The total volume of all the 6 lakes in this catchment is 73Mm^3 . Hence there is an overland surplus flow of 77Mm^3 which cannot flow to downstream due to disruption of natural drainage (removal of lakes and blockage of storm water drains) resulting in flooding (even during normal rainfall).

Similar analyses for the Madivala and Bellandur drainage network revealed that encroachment and conversion has resulted in the loss of connectivity between Yelchenhalli kere and Madivala (Figure 7). Madivala – Varthur catchment has 14 lakes – Venkatapura, Yellakunte, Bandepalya, Begur Doddakere, Madivala, Hulimavu, Marenahalli, Govindanaikana kere, Tank north of Doresanipalya, Gittigere, and Vaddarpalya. The total rainfall yield is 247Mm^3 , percolated water is 97Mm^3 and the remaining water 150Mm^3 flows as overland flow and storage in lakes. The total volume of all the lakes considering 1m depth is 110Mm^3 , resulting in the excess of 40Mm^3 from the catchment leading to artificial floods.

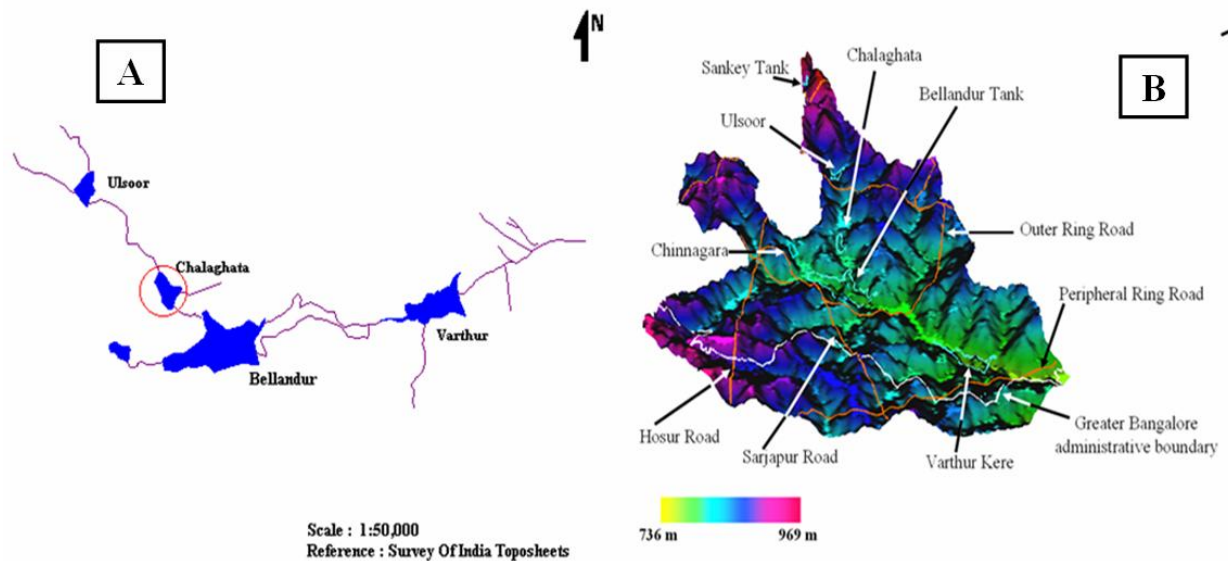


Figure 6. Ulsoor–Bellandur–Varthur (a) drainage network and catchment, (b) lakes overlaid on 10 m DEM showing their missing interconnectivity

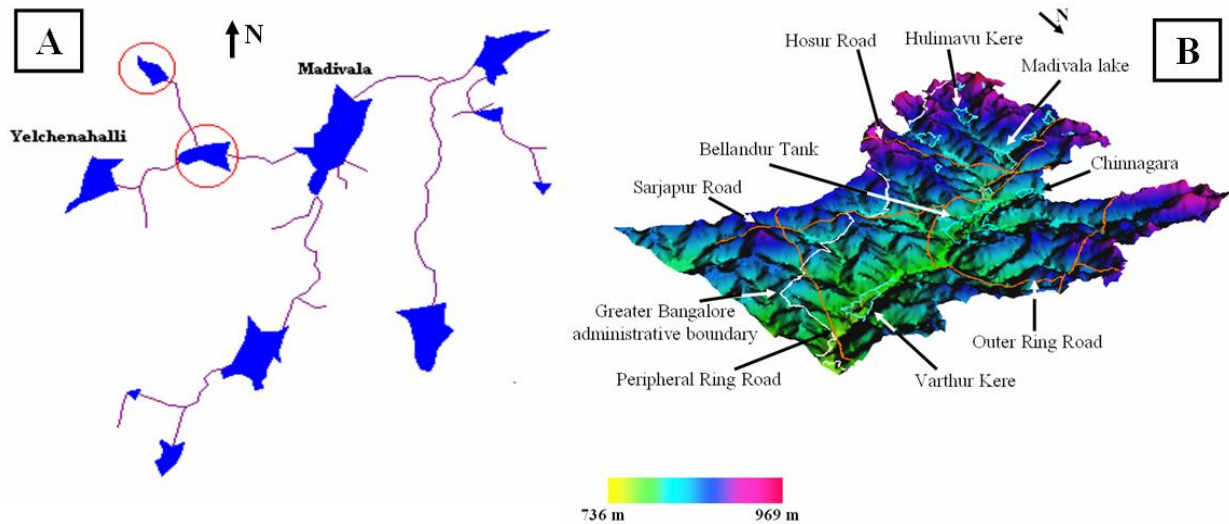


Figure 7. Madivala–Bellandur–Varthur (a) drainage network and catchment, (b) lakes overlaid on 10 m DEM showing their missing interconnectivity

Increased peak discharge and higher frequency of floods are the consequences of urbanization. As land is converted from fields or woodlands to built-up areas, roads, and parking lots, it loses its ability to absorb rainfall. Urbanization has increased runoff two to six times over what would occur on natural terrain in some pockets of Bangalore. During periods of urban flooding, streets become swift moving rivers, while low lying residential areas and basements become death traps as they fill with water. Conversion of water bodies to residential layouts has further compounded the problem in an undulating terrain.

Flooding in urban areas causes large damage to buildings and other public and private infrastructure (evident during 1997, 2002 and 2007). Besides, street flooding can limit or completely hinder the functioning of traffic systems and has indirect consequences such as loss of business and opportunity. The expected total damage, direct and indirect monetary damage costs as well as possible social consequences is related to the physical properties of the flood, i.e. the water level above ground level, the extent of flooding in terms of water volume escaping from or not being entering the drainage system, and the duration of flooding.

Also, due to increased paved surfaces and concentrated human activities the magnitude of the difference in observed ambient air temperature between urban pockets (artificial land surface) and the regions covered with vegetation (natural areas), is ascribed as the urban heat island effect. The urban heat island effect results in increased local atmospheric and surface temperatures in urban pockets compared to the surrounding open spaces, etc. Specifically, surface and atmospheric temperatures are increased by anthropogenic heat discharge due to energy consumption, increased land surface coverage by artificial materials having high heat capacities and conductivities, increased vehicular and industrial emissions and the associated decreases in vegetation and water-pervious surfaces, which reduce surface temperature through evapotranspiration. An attempt is made here to understand the implications of land cover changes on local climate.

Enhanced Land Surface Temperature (LST) and Land Cover

Land cover was computed through NDVI (Normalized Difference Vegetation Index) from visible Red (0.63 – 0.69 μm) and NIR (0.76 – 0.90 μm) bands of Landsat ETM+ (2000) to understand its role in LST. LST is computed using Landsat ETM+ thermal band 6.1 (low gain). Digital number (DN) of Landsat ETM+ was first converted into spectral radiance L_{ETM} using equation 1, and then

converted to at-satellite brightness temperature (i.e., black body temperature, $T_{ETMSurface}$), under the assumption of uniform emissivity ($\epsilon \approx 1$) using equation 2:

$$L_{ETM} = 0.0370588 \times DN + 3.2 \quad \dots(\text{Equation 1})$$

$$T_{ETMSurface} = K_2 / \ln (K_1 / L_{ETM} + 1) \quad \dots(\text{Equation 2})$$

where,

$T_{ETMSurface}$ is the effective at-satellite temperature in Kelvin, L_{ETM} is spectral radiance in watts/(meters squared x ster x μm); and K_1 and K_2 are pre-launch calibration constants. For Landsat-7 ETM+, $K_2 = 1282.71$ K and $K_1 = 666.09 \text{ mWcm}^{-2}\text{sr}^{-1}\mu\text{m}^{-1}$ were used (http://ftpwww.gsfc.nasa.gov/IAS/handbook/handbook_htmls/chapter11/chapter11.html). The emissivity corrected land surface temperatures T_s were finally computed by equation 3:

$$T_s = \frac{T_B}{1 + (\lambda \times T_B / \rho) \ln \epsilon} \quad \dots (\text{Equation 3})$$

where, λ is the wavelength of emitted radiance for which the peak response and the average of the limiting wavelengths ($\lambda = 11.5 \mu\text{m}$) (Markham and Barker, 1985) were used, $\rho = h \times c / \sigma$ ($1.438 \times 10^{-2} \text{ mK}$), $\sigma = \text{Stefan Boltzmann's constant}$ ($5.67 \times 10^{-8} \text{ Wm}^{-2}\text{K}^{-4} = 1.38 \times 10^{-23} \text{ J/K}$), $h = \text{Planck's constant}$ ($6.626 \times 10^{-34} \text{ Jsec}$), $c = \text{velocity of light}$ ($2.998 \times 10^8 \text{ m/sec}$), and ϵ is spectral emissivity.

The minimum and maximum temperatures from ETM+ data were 13.49 and 26.32 with a mean of 21.75 and SD of 2.3. Figure 8 shows the LST map and NDVI of Greater Bangalore and Table 2 lists the respective LST and NDVI values. Analysis of LST shows a variation from 23.09°C (dense urban), 22.4°C (open ground) to 22.14°C (mixed urban), 19.27°C (for area under vegetation) and 19.57°C (water bodies) indicating the enhanced temperatures in urbanized regions (Table 2). Figure 9 illustrates temperatures with population density for 100 wards of city conforming heat island phenomenon with the increase in built-up area consequent to the increase in population density. Temporal analysis showed a linear growth of 466% in number of urban pixels from 1973 to 2007 and a decline of 61% in the number of water bodies with a 63% decrease in vegetation cover. Similarly during 1992 to 2007, the increase in built-up pixels was 63% while vegetation and water bodies decline by 45 and 43.8% respectively. Correlation analysis of LST with built-up areas and vegetation shows relationships of increasing LST with increase in built-up areas and decrease of vegetation and water bodies (Table 2).

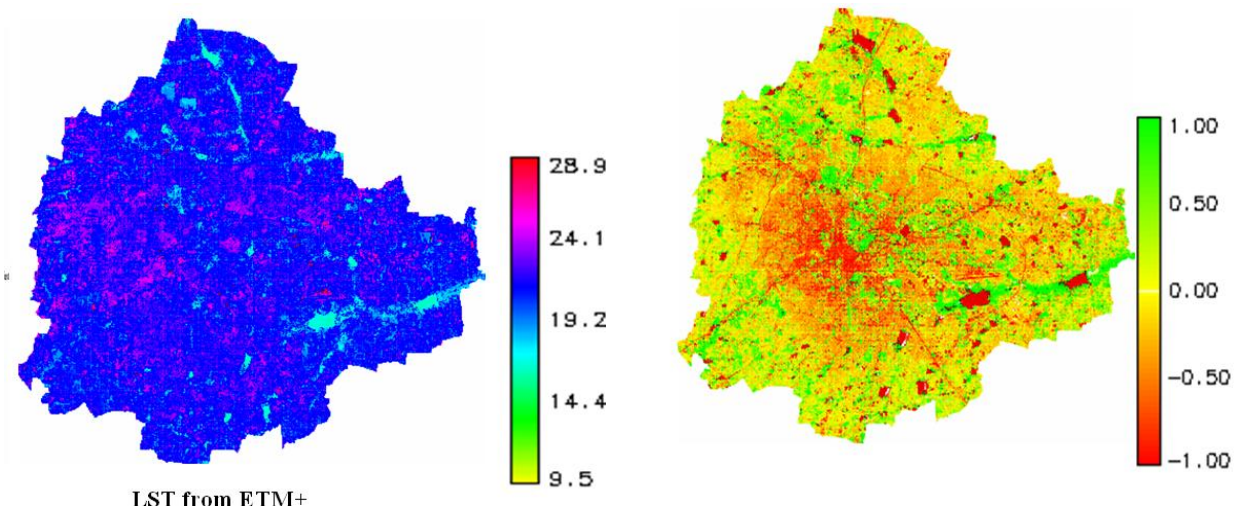


Figure 8. Land surface temperature (LST) and NDVI

Table 2. LST and NDVI

| Landuse | LST Mean \pm SD | NDVI Mean \pm SD | r |
|---------------|----------------------|-----------------------|---------|
| Dense builtup | 23.09 \pm 1.16 | -0.2904 \pm 0.395 | -0.7771 |
| Mixed builtup | 22.14 \pm 1.06 | -0.138 \pm 0.539 | -0.6834 |
| Vegetation | 19.27 \pm 1.59 | 0.3969 \pm 0.404 | -0.8500 |
| Open Ground | 22.40 \pm 1.97 | -0.0193 \pm 0.164 | -0.6319 |
| Water Bodies | 19.57 \pm 1.72 | -0.301 \pm 0.47 | 0.2319 |

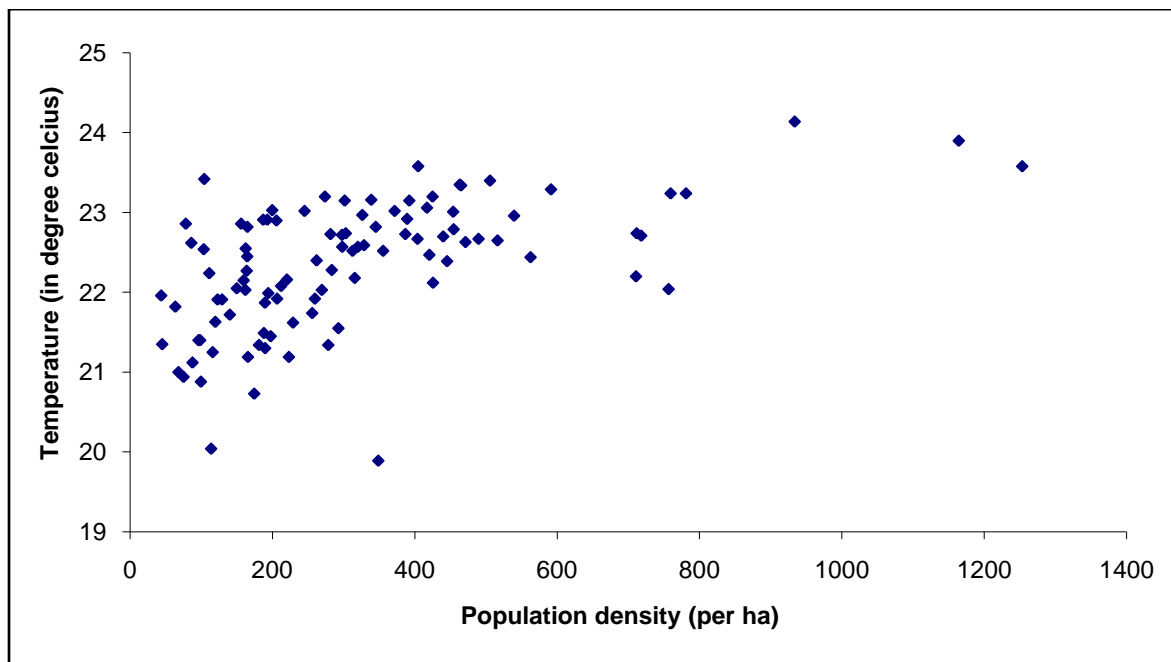


Figure 9: Population density and land surface temperature

Recommendations

The uncoordinated pattern of urban growth happening in Greater Bangalore could be attributed to a lack of good governance and decentralized administration evident from lack of coordination among many para-statal agencies, which has led to unsustainable use of the land and other resources.

Failure to deal with water as a finite resource is leading to the unnecessary destruction of lakes and marshes that provide us with water. This failure in turn is threatening all options for the survival and security of plants, animals, humans, etc. There is an urgent need for:

- **Restoring and conserving the actual source of water** - the water cycle and the natural ecosystems that support it - are the basis for sustainable water management

- **Reducing the environmental degradation that is preventing us from reaching goals** of good public health, food security, and better livelihoods world-wide
- **Improving the human quality of life** that can be achieved in ways while maintaining and enhancing environmental quality
- **Reducing greenhouse gases to avoid the dangerous effects of climate change** is an integral part of protecting freshwater resources and ecosystems.

A comprehensive approach to water resource management is needed to address the myriad water quality problems that exist today from non-point and point sources as well as from catchment degradation. Watershed-based planning and resource management is a strategy for more effective protection and restoration of aquatic ecosystems and for protection of human health. The watershed approach emphasizes all aspects of water quality, including chemical water quality (e.g., toxins and conventional pollutants), physical water quality (e.g., temperature, flow, and circulation), habitat quality (e.g., stream channel morphology, substrate composition, riparian zone characteristics, catchment land cover), and biological health and biodiversity (e.g., species abundance, diversity, and range).

Conservation strategies should focus on conservation and maintaining the ecological health of watersheds and aquatic ecosystems so as to (Ramachandra, T.V., 2002):

- Maintain and conserve the distribution, diversity, and complexity of watershed and landscape-scale features to ensure protection of the aquatic systems to which species, populations, and communities are uniquely adapted.
- Maintain and conserve spatial and temporal connectivity within and between watersheds. Lateral, longitudinal, and drainage network connections include flood plains, wetlands, up slope areas and headwater tributaries. These lineages must provide chemically and physically unobstructed routes to areas critical for fulfilling life history requirements of aquatic and riparian-dependent species.
- Maintain and restore the physical integrity of the aquatic system, including shorelines, banks, and bottom configurations.
- Maintain and preserve water quality necessary to support healthy riparian, aquatic, and wetland ecosystems. Water quality must remain in the range that maintains the biological, physical, and chemical integrity of the system and benefits survival, growth, reproduction, and migration of individuals composing aquatic and riparian communities.
- Maintain the sediment regime under which an aquatic ecosystem evolved. Elements of the sediment regime include the timing, volume, rate, and character of sediment input, storage, and transport.
- Maintain in-stream flows sufficient to create and sustain riparian, aquatic, and wetland habitats and to retain patterns of sediment, nutrient, and wood routing (i.e., movement of woody debris through the aquatic system). The timing, magnitude, duration, and spatial distribution of peak, high, and low flows must be protected.
- Maintain the timing, variability, and duration of flood plain inundation and water table elevation in meadows and wetlands.
- Maintain and conserve the species composition and structural diversity of plant communities in riparian zones and wetlands to provide adequate summer and winter thermal regulation, nutrient filtering, appropriate rates of surface erosion, bank erosion, and channel migration, and to supply amounts and distributions of coarse woody debris sufficient to sustain physical complexity and stability.
- Maintain and conserve habitat to support well-distributed populations of native plant, invertebrates, and vertebrate riparian-dependent species.
- Aquatic ecosystem conservation and management require collaborated research involving natural, social, and inter-disciplinary study aimed at understanding the various components, such as monitoring of water quality, socio-economic dependency, biodiversity, and other activities, as an indispensable tool for formulating long term conservation strategies (Ramachandra, et al., 2002). This requires multidisciplinary-trained professionals who can spread the understanding of the ecosystem's importance

at local schools, colleges, and research institutions by initiating educational programs aimed at raising the levels of public awareness and comprehension of aquatic ecosystem restoration, goals, and methods. Actively participating schools and colleges in the vicinity of the water bodies may value the opportunity to provide hands-on environmental education which could entail setting up laboratory facilities at the site. Regular monitoring of water bodies (with permanent laboratory facilities) would provide vital inputs for conservation and management.

- Effective aquatic ecosystem management requires sound data, information and knowledge, including both data on surface and groundwater (quantity and quality) and social and economic data. Collection and processing of relevant data, easy accessibility and broad dissemination are eminent tasks of river basin management. To increase policy relevance, data should be aggregated into meaningful information, for example in the form of indicators and systems for benchmarking. Compliance monitoring (reporting, reviewing and evaluating) is very important for promoting the implementation of plans.
- Sustainable aquatic resources development and management depends mainly on proper planning, implementation, operation and maintenance, which is possible with Geographic Information System (GIS) and RS techniques, complement and supplement ground data collection in various facets of different kinds of water resources projects. The synoptic large area repetitive coverage provided by satellite sensors provide appropriate database.
- To support strategic planning, methods for analytical support should be developed that:
 - ✓ cover the whole basin and all significant impacts
 - ✓ specifically consider the socio-economic processes that affect the basin
 - ✓ predict the socio-economic effects of alternative strategies
 - ✓ present the issues in such a way that people can understand them

Integrated aquatic ecosystem management requires proper study, sound understanding and effective management of water systems and their internal relations (groundwater, surface water and return water; quantity and quality; biotic components; upstream and downstream). The water systems should be managed as part of the broader environment and in relation to socio-economic demands and potentials, acknowledging the political and cultural context. The water itself should be seen as a social, environmental, and economic resource, and each of these three aspects must be represented in the political discourse. To implement the general principles of the integrated aquatic ecosystem management requires a cyclic policy development approach. Such an approach would include the following steps: assessment of institutions, needs and resources, planning, implementation, compliance monitoring and evaluation.

Conclusion

Pattern classifiers along with the advances in geo-informatics, coupled with the availability of higher spatial, spectral and temporal resolution data help in extracting spatial features of interest like land cover classes such as water. Water bodies influence biophysical processes and energy exchanges between the atmosphere and the land surface as required by local and regional-scale climate and ecosystem process models. In this context, an important application of pattern classifiers would be to estimate accurate temporal land cover maps that are useful in monitoring the status of water bodies. The analysis showed that out of 265 water bodies in greater Bangalore in 1972, only 110 exist in 2007. The analysis showed a linear growth of 466% in number of urban pixels from 1973 to 2007 and a decline of 61% in the number of water bodies with a 63% decrease in vegetation cover in Greater Bangalore. Very few of them are in good condition and most of them are victims of encroachment, dumping yards and mismanagement. Appropriate policy decisions, interventions, and holistic approaches are required to restore them from degradation and achieve a sustainable environment.

Acknowledgements

We thank the Ministry of Science and Technology, Government of India and Indian Institute of Science for financial assistance and infrastructure support.

References

- Carper, W.J., Lillesand, T.M., & Kiefer, R.W. (1990). The use of intensity–hue–saturation transformation for merging SPOT panchromatic and multi-spectral image data. *Photogrammetric Engineering and Remote Sensing*, 56(4), 459-467.
- Czarnik-Matuszewicz, B., & Pilorz, S. (2006). Study of the temperature-dependent near-infrared spectra of water by two-dimensional correlation spectroscopy and principal components analysis. *Vibrational Spectroscopy*, 40, 235-245.
- Duda, R. O., Hart, P. E., & Stork, D. G. (2000). *Pattern classification*. New York: Wiley.
- French, R. H., Miller, J. J., Dettling, C., & Carr, J. R. (2006). Use of remotely sensed data to estimate the flow of water to a playa lake. *Journal of Hydrology*, 325, 67-81.
- Fukushima, K. (1988). A neural network for visual pattern recognition. *IEEE Computer*, 21(3), 65-74.
- Gori, M., & Scarselli, F. (1998). Are multilayer perceptrons adequate for pattern recognition and verification? *IEEE Transactions on Pattern Analysis and Machine Intelligence*, 20(11), 1121-1132.
- Kevin, W., & El Asmar, H. M. (1999). Monitoring changing position of coastlines using thematic mapper imagery, an example from the Nile Delta. *Geomorphology*, 29(1), 93-105.
- Kwan, H. K., & Cai, Y. (1994). A fuzzy neural network and its application to pattern recognition. *IEEE Transactions on Fuzzy Systems*, 2(3), 185-193.
- Lee, C. H. N., Liu, A., & Chen, W. S. (2006). Pattern discovery of fuzzy time series for financial prediction. *IEEE Transactions on Knowledge and Data Engineering*, 18(5), 613-625.
- Lillesand, T.M., & Kiefer, R. W. (2002). *Remote sensing and image interpretation* (4th ed.). New York: Wiley.
- Ramachandra, T.V. (2002). Restoration and management strategies of wetlands in developing countries. *Electronic Green Journal*, 15. Retrieved November 24, 2007, from <http://egj.lib.uidaho.edu/index.php/egj/article/view/2839/2797>
- Ramachandra, T.V., Kiran, R., & Ahalya, N. (2002). *Status, conservation and management of wetlands*. New Delhi: Allied Publishers.
- Sudhira H.S., Ramachandra T.V., & Bala Subramanya, M.H. (2007). City profile: Bangalore. *Cities*, 124(4), 379-390.
- Wilson, P. A. (1997). Rule-based classification of water in Landsat MSS images using the variance filter. *Photogrammetric Engineering & Remote Sensing*, 63(5), 485-491.
- Yamano, H., Shimazaki, H., Matsunaga, T., Ishoda, A., McClennen, C., Yokoki, H., Fujita, K., Osawa, Y., & Kayanne, H. (2006). Evaluation of various satellite sensors for waterline

extraction in a coral reef environment: Majuro Atoll, Marshall Islands. *Geomorphology*, 82(3-4), 398–411.

Electronic Green Journal, Issue 26, Spring 2008
ISSN: 1076-7975

Appendix A.
Mathematical description of Principal Component Analysis

Let m (4 in case of MODIS as used here) be the total number of bands used in the analysis. To every pixel, we associate a four-dimensional feature vector with components corresponding to the grey values of the four bands. The sample mean of the pixels is defined by

$$\mu = \frac{1}{n} \sum_{i=1}^n \mathbf{x}_i \quad \dots \quad (\text{Equation 4})$$

where, μ is the mean of the feature vector, \mathbf{x}_i is the feature vector of the i th pixel and n is the total number of pixels. The covariance matrix is defined as

$$\sum_x = E\{(x - \mu)(x_n - \mu)^t\} \quad \dots \quad (\text{Equation 5})$$

In equation 5, the superscript 't' denotes vector transpose. An unbiased estimate of the sample covariance matrix \mathbf{C} is given by

$$C = \frac{1}{n-1} \sum_{i=1}^n (x_i - \mu)(x_i - \mu)^t \quad \dots \quad (\text{Equation 6})$$

Next, the eigen values and eigen vectors of the matrix \mathbf{C} were computed by solving the equation

$$(\mathbf{C} - \lambda_i * \mathbf{I}) * \mathbf{e}_i = 0 \quad \dots \quad (\text{Equation 7})$$

where $\mathbf{e}_i = (a_1, a_2, \dots, a_m)^t$ is the eigenvector corresponding to the eigen values λ_i and \mathbf{I} is the identity matrix. The eigen values λ_i , were determined by solving the characteristic equation

$$|\mathbf{C} - \lambda * \mathbf{I}| = 0 \quad \dots \quad (\text{Equation 8})$$

A new coordinate system is formed by normalised eigen vectors of the covariance (or correlation) matrix \mathbf{C} . The mapping of each feature vector $\mathbf{x} = (x_1, x_2, x_3, \dots, x_m)$ on the i^{th} principal component is given by:

$$f_i = \mathbf{x} * \mathbf{e}_i = x_1 * e_1^i + x_2 * e_2^i + \dots + x_m * e_m^i \quad \dots \quad (\text{Equation 9})$$

Appendix B.
Mathematical description of RGB-HIS fusion

The 3 low resolution bands (considered as blue (band 1), green (band 2) and red (band 3)) are transformed to the IHS using equations 10, 11 and 12.

$$\begin{pmatrix} I \\ V_1 \\ V_2 \end{pmatrix} = \begin{pmatrix} \frac{1}{3} & \frac{1}{3} & \frac{1}{3} \\ \frac{1}{\sqrt{6}} & \frac{1}{\sqrt{6}} & -\frac{2}{\sqrt{6}} \\ \frac{1}{\sqrt{2}} & -\frac{1}{\sqrt{2}} & 0 \end{pmatrix} \begin{pmatrix} R \\ G \\ B \end{pmatrix} \quad \dots \quad \text{(Equation 10)}$$

R, G and B corresponds to band 1, 2 and 3

$$H = \tan^{-1} \left(\frac{V_2}{V_1} \right) \quad \dots \quad \text{(Equation 11)}$$

$$S = \sqrt{V_1^2 + V_2^2} \quad \dots \quad \text{(Equation 12)}$$

Here V_1, V_2 are the intermediate variables.

I is replaced with the high spatial resolution image. Then, the fused images are obtained by performing an inverse transformation of IHS back to the original RGB as given in equation 13.

$$\begin{pmatrix} R \\ G \\ B \end{pmatrix} = \begin{pmatrix} 1 & \frac{1}{\sqrt{6}} & \frac{1}{\sqrt{2}} \\ 1 & \frac{1}{\sqrt{6}} & -\frac{1}{2} \\ 1 & -\frac{2}{\sqrt{6}} & 0 \end{pmatrix} \begin{pmatrix} I \\ V_1 \\ V_2 \end{pmatrix} \quad \dots \quad \text{(Equation 13)}$$

Appendix C.
Mathematical description of K-means Clustering

We knew the initial 4 clusters (builtup, vegetation, wetlands and others) but the probability $p(x|\omega_k)$ was unknown where x is the feature vector and ω_k is the k th class. In many situations, the form of the $p(x|\omega_k)$ is assumed to be normal, and therefore the distribution $p(x|\omega_k)$ is completely characterised by the parameter $\Theta = (\mu, \Sigma)$ where μ is the sample mean and Σ is the covariance matrix.

Randomly 4 pixels were selected each of which initially represents a class mean $\hat{\mu} (\mu_1, \mu_2, \dots, \mu_k)$. For each of the remaining pixels, a pixel was assigned to the class to which it was closest to its mean based on the similarity function – the Euclidean distance $\|x - \hat{\mu}_k\|^2$ between the pixel x and the class mean μ_k .

New means were computed for each class. The process was iterated until the criterion function converged. The square-error criterion is

$$E = \sum_{k=1}^4 \sum_{x_k \in C_k} |x_k - \hat{\mu}_k|^2 \quad \dots \quad \text{(Equation 14)}$$

where, E is the sum of the square error for all pixels in the data set. The distance from the pixel to its cluster centre is squared, and the distances are summed making the 4 clusters as compact as possible terminating at a local optimum.

Appendix D.
Mathematical description of maximum-likelihood classifier

The prior probability $P(\omega_k)$ for the k th class which is the proportion of the number of pixels in that class to the total number of pixels and the covariance matrix Σ_k were computed.

The justification for choosing the sample mean and covariance estimates for the true mean and covariance is as follows.

We had k samples according to the classes given by D_1, \dots, D_k (builtup, vegetation, waterbodies and others, hence $k = 4$) where the samples in D_k were i.i.d (independent and identically distributed) random variables with probability $p(x|\omega_k)$ having known parametric form, therefore they could be determined uniquely by the value of a parameter vector Θ_k . Because of dependence of $p(x|\omega_k)$ on Θ_k , $p(x|\omega_k)$ can be written as $p(x|\omega_k, \Theta_k)$. The classes information $\hat{\mu} (\mu_1, \mu_2, \dots, \mu_k)$ obtained from earlier steps can be used to obtain estimates for unknown parameter vectors $\Theta_1, \Theta_2, \dots, \Theta_k$. Assuming that samples in D_i give no information about Θ_k if $i \neq k$, i.e., parameters for the different classes are functionally independent. So,

$$p(D|\theta) = \prod_{k=1}^n p(x_k|\theta) \quad \dots \quad \text{(Equation 15)}$$

Let Θ denote the p -component vector $\Theta = (\Theta_1, \dots, \Theta_p)^t$ and let $\nabla \theta$ be the gradient operator, so $l(\Theta) \equiv \ln p(D|\Theta)$ that maximizes the log likelihood is $\hat{\theta} = \text{argmax} l(\theta)$ over Θ .

$$\text{Now } l(\theta) = \sum_{k=1}^n \ln p(x_k | \theta) \quad \dots \quad (\text{Equation 16})$$

$$\text{and } \nabla_{\theta} l = \sum_{k=1}^n \nabla_{\theta} \ln p(x_k | \theta) \quad \dots \quad (\text{Equation 17})$$

Thus, the maximum likelihood estimates for Θ is obtained from the set of p equations, $\nabla_{\theta} l = 0$. A solution to Θ could represent a global, local maximum or minimum out of which one represents a true maximum, which is confirmed by the calculating the second derivatives.

In our case, μ_k and Σ_k are unknown, so this constitute the components of the parameter vector Θ . Considering the univariate case, with $\Theta_1 = \mu$ and $\Theta_2 = \sigma^2$, the log-likelihood of a single point is

$$\ln p(x_k | \theta) = -\frac{1}{2} \ln 2\pi\theta_2 - \frac{1}{2\theta_2} (x_k - \theta_1)^2 \quad \dots \quad (\text{Equation 18})$$

and its derivative is

$$\nabla_{\theta} l = \nabla_{\theta} \ln p(x_k | \theta) = \begin{bmatrix} \frac{1}{\theta_2} (x_k - \theta_1)^2 \\ -\frac{1}{2\theta_2} + \frac{(x_k - \theta_1)^2}{2\theta_2^2} \end{bmatrix} \quad \dots \quad (\text{Equation 19})$$

Applying the full log-likelihood and rearranging the terms, the maximum-likelihood estimate for multivariate case on substituting the $\hat{\mu} = \hat{\theta}_1$ and $\hat{\sigma}^2 = \hat{\theta}_2$ is

$$\hat{\mu} = \frac{1}{n} \sum_{k=1}^n x_k \quad \dots \quad (\text{Equation 20})$$

$$\hat{\Sigma} = \frac{1}{n} \sum_{k=1}^n (x_k - \mu')(x_k - \mu')^t \quad \dots \quad (\text{Equation 21})$$

The sample mean and covariance are taken as the maximum-likelihood estimate for the true mean vector and covariance matrix. The covariance matrices are assumed to be different for each category. So the maximum-likelihood quadratic discriminant analysis classifier is

$$g_i(x) = x^t W_i x + w_i^t x + \omega_{i0} \quad \dots \quad (\text{Equation 22})$$

where

$$W_i = -\frac{1}{2} \sum_i^{-1} \dots \quad (\text{Equation 23})$$

$$w_i = -\frac{1}{2} \sum_i^{-1} \mu_i \dots \quad (\text{Equation 24})$$

$$\omega_{i0} = -\frac{1}{2} \mu_i^t \sum_i^{-1} \mu_i - \frac{1}{2} \ln | \sum_i | + \ln P(\omega_i) \dots \quad (\text{Equation 25})$$

The values of mean $\hat{\mu}$, covariance $\hat{\Sigma}$ and prior probability $P(\omega_i)$ are substituted in the discriminant function as given by equation 19. A pixel is assigned to a particular class for which it has the maximum probability. This provides the unsupervised classified image with the k classes.

.....

T.V. Ramachandra <cestvr@ces.iisc.ernet.in>, Energy & Wetlands Research Group,
 Centre for Ecological Sciences, Indian Institute of Science, Bangalore – 560 012, INDIA
 Tel : 91-80-23600985/22932506/22933099, Fax : 91-80-23601428/23600085/23600683[CES-TV
 R].

Uttam Kumar <uttam@ces.iisc.ernet.in>, Centre for Sustainable Technologies, Indian Institute of
 Science, Bangalore, India.